Gradients of Column CO_2 across North America from the NOAA Global Greenhouse Gas Reference Network

Xin Lan[1, 2], Pieter Tans[1], Colm Sweeney[1, 2], Arlyn Andrews[1], Andrew Jacobson[1, 2], Molly Crotwell[1, 2], Edward Dlugokencky[1], Jonathan Kofler[1, 2], Patricia Lang[1], Kirk Thoning[1], Sonja Wolter[1,2]

[1]1National Oceanic and Atmospheric Administration, Earth System Research Laboratory, Boulder, 80303, Colorado, USA

[2] University of Colorado, Cooperative Institute for Research in Environmental Sciences, Boulder, 80309, Colorado, USA

Correspondence to: Xin.Lan (xin.lan@noaa.gov)

Abstract. This study analyzes seasonal and spatial patterns of column carbon dioxide (CO_2) over North America calculated from aircraft and tall tower measurements from the NOAA Global Greenhouse Gas Reference Network from 2004 to 2014. Consistent with expectations, gradients between the eight regions studied are larger below 2 km than above 5 km. The 11-year mean CO_2 dry mole fraction (XCO_2) in the column below ~330 hPa (~ 8 km above sea level) from NOAA's CO_2 data assimilation model, CarbonTracker (CT2015), demonstrates good agreement with those calculated from calibrated measurements on aircraft and towers. Total column XCO_2 was attained by combining modeled CO_2 above 330 hPa from CT2015 with the measurements. We find large spatial gradients of total column XCO_2 during June to August, with north and northeast regions having ~3 ppm stronger summer drawdown (peak to valley amplitude in seasonal cycle) than the south and southwest regions. The long-term averaged spatial gradients of total column XCO_2 across North America show a smooth pattern that mainly reflects the large-scale circulation . We have conducted a CarbonTracker experiment to investigate the impact of Eurasian long-range transport. The result suggests that the large summer time Eurasian boreal flux contributes about half of the north-south column XCO_2 gradient across North America. Our results confirm that continental-scale total column XCO_2 gradients simulated by CarbonTracker are realistic and can be used to evaluate the credibility of some spatial patterns from satellite retrievals, such as the long term average of growing-season spatial patterns from satellite retrievals reported for Europe which show larger spatial difference (~ 6 ppm) and scattered hot spots.

1 Introduction

Atmospheric measurements of carbon dioxide (CO_2) from ground and airborne platforms have greatly increased our knowledge of the global carbon cycle. Observations of CO_2, including the NOAA Global Greenhouse Gas Reference Network (GGGRN), initially emphasized ground-based measurements. These observations, started by C.D. Keeling, have monitored the CO_2 trend on both regional and global scales for over 50 years (e.g., Keeling and Rakestraw, 1960; Tans et al., 1989). In addition, the frequency and spatial distribution of airborne measurements have increased rapidly in the last two decades, providing important information about horizontal and vertical variability of atmospheric CO_2 (e.g., Gerbig et al., 2003; Choi et al., 2008; Biraud et al., 2013). Routine aircraft

36 measurements from the NOAA/ESRL GGGRN monitor the large-scale distributions of a suite of trace gases,
37 including CO_2, under the influence of continental processes (Sweeney et al., 2015). A very successful approach has
38 been to employ commercial aircraft as a platform for CO_2 measurements, such as Japan's CONTRAIL
39 (Comprehensive Observation Network for TRace gases by AIrLiner) project, which has provided valuable
40 information for CO_2 in the high troposphere and lower stratosphere (Machida et al., 2002; Machida et al., 2008).
41 Vertical profiles of atmospheric CO_2 reflect the combined influences of surface fluxes and atmospheric mixing.
42 Vertical profiles are particularly useful for evaluating vertical mixing in atmospheric transport models that are used
43 for inverse modeling (e.g. Stephens et al., 2007) to derive estimates of regional- to continental-scale CO_2 sources
44 and sinks (e.g., Tans et al., 1990; Gurney et al., 2002; Gurney et al., 2004; Ciais et al., 2010;).

45 While CO_2 sources and sinks are well constrained at the global scale by global mass balance, it remains
46 challenging to accurately resolve CO_2 sources and sinks at regional to continental-scale, the apportionment of which
47 depends on relatively minor variations of the observed spatial and temporal patterns of CO_2. When averaging over a
48 few months and longer the largest portion of the variations over continents results from hemispheric-scale terrestrial
49 uptake/emissions (photosynthesis)/respiration) and fossil fuel emissions, while regional net fluxes can make a
50 relatively small contribution to the signal. For example, a simple mass balance argument shows that all U.S. CO_2
51 emissions from fossil fuel burning (~1.4 Pg yr^{-1}) create a total column enhancement of only 0.6 ppm on average in
52 air parcels over the East Coast compared to the West Coast and Gulf Coast if we assume an average of 5 days for the
53 winds to flush the contiguous U.S. (~8×10^{12} m^2).

54 With careful calibration, air handling, and analysis, the uncertainties of in-situ measurements are less than 0.1
55 ppm. However, in-situ observation networks are sparse in global and regional coverage. Remote sensing data
56 radically increase the number of observations and capture under-sampled regions. It could have a valuable impact on
57 our understanding of the carbon cycle. However, both the precision and the potential of even very small systematic
58 biases in remote sensing measurements need to be carefully evaluated, especially those that depend on regional and
59 seasonal conditions. Vertical profiles from in-situ CO_2 measurements have been used to evaluate ground-based total
60 column XCO_2 (the "X" stands for dry mole fraction) determinations, such as those from the Total Carbon Column
61 Observing Network (TCCON) (Washenfelder et al., 2006; Wunch et al., 2010; Messerschmidt et al., 2011; Tanaka
62 et al., 2012). The uncertainty of TCCON total column CO_2 is reported to be 0.4 ppm (1σ) after comparison to
63 aircraft measurements (Wunch et al., 2010). Vertical profiles are also used to evaluate other satellite retrievals of
64 total column XCO_2, such as those from the Tropospheric Emission Spectrometer (TES)(Kulawik et al., 2013) and
65 the Greenhouse Gases Observing SATellite (GOSAT) (Inoue et al., 2013, 2016; Saitoh et al., 2016). Satellite
66 retrieval products have known and unknown biases (due to errors in spectroscopy, viewing geometry, spatial
67 differences in clouds and aerosols, surface albedo, etc.) that can result in false horizontal gradients in total column
68 XCO_2 for inverse estimates of sources (Miller et al., 2007; Crisp et al., 2012; Feng et al., 2016). After correction for
69 known biases, the mean GOSAT total column CO_2 (NIES retrievals) biases range between -2.09 to 3.37 ppm (mean
70 = 0.11 ppm, S.D.= 1.11 ppm; 20 out of 27 stations show biases lower than 1 ppm) across different aircraft sites over
71 land when compared with aircraft-based total column XCO_2 (Inoue et al.,2016). The Orbiting Carbon Observatory-
72 2 (OCO-2) retrieval of total column XCO_2 was estimated to have a mean difference less than 0.5 ppm from TCCON,

73 with RMS differences typically below 1.5 ppm after bias correction (Wunch et al., 2016). The overall uncertainty of

74 satellite retrievals is relatively large compared with the total column XCO_2 calculated from in-situ measurements.

75 Total column XCO_2 calculated from vertical profiles from the Japanese CONTRAIL project (Machida et al., 2008)

76 and from the NOAA Carbon Cycle and Greenhouse Gas aircraft program (Sweeney et al., 2015) complemented with

77 simulated profiles from a chemistry–transport model above the maximum altitude of the data have uncertainty less

78 than 1 ppm (Miyamoto et al., 2013). The smaller uncertainty of the in situ-based total column XCO2 suggests that

79 they can be used to evaluate satellite retrievals of column averaged CO_2. Since aircraft profiles co-located with

80 satellite retrievals are rare, it is useful to consider the statistics of total column XCO_2 fields derived from repeated

81 aircraft profiles over particular locations.

82   The effect of satellite column averaging kernels and a priori profiles when comparing aircraft-based column

83 XCO_2 with GOSAT retrievals has been assessed by Inoue et al. (2013). For the case considered, application of the

84 averaging kernel and a priori profile to simulate total column XCO_2 was generally within $\pm$ 0.1 ppm of the density

85 weighted total column, suggesting that the averaging kernels can only account for small part of the overall

86 uncertainty of the GOSAT total column XCO_2 (Inoue et al., 2013).

87   Transparent and objective estimates of CO_2 sources and sinks derived from atmospheric measurements are

88 essential for validating emissions reduction efforts and other mitigation policies, and for lowering the uncertainties

89 of carbon cycle-climate feedbacks. The latter are major ambiguities in predicting future climate, such as potential

90 uncontrolled CH_4 and CO_2 emissions from warming permafrost in Arctic regions. Satellite retrievals of total column

91 XCO_2 can significantly improve estimates of sources and sinks only if they are sufficiently precise and accurate (

92 Houweling et al., 2004; Chevallier et al., 2014), meaning that even very small systematic errors (biases) must be

93 eliminated. Here, we analyze the spatial and temporal variability of column CO_2 over North America using well-

94 calibrated CO_2 measurements from aircraft and tall tower, and we use model results from NOAA's CarbonTracker,

95 version CT2015 (Peters et al. 2007, with updates documented at http://carbontracker.noaa.gov) to investigate the

96 primary drivers of variability in total column XCO_2. The aircraft data enable direct analysis of column CO_2

97 characteristics, which is the fundamental step for accurate apportionment of sources and sinks. This study focuses on

98 long-term averaged column CO_2 gradients and the contributions of different vertical layers to the total column

99 variability. It can serve as a reference for evaluating regional and seasonal biases of current and future column CO_2

100 retrievals from both ground and satellite platforms.

101 **2 Methods**

102 **2.1 Aircraft and tall tower sampling**

103 Aircraft sampling in the NOAA GGGRN intends to provide vertical profiles of long-lived trace gases to capture

104 their seasonal and interannual variability. The aircraft sampling system consists of 12 borosilicate glass flasks in

105 each programmable flask package (PFP), a stainless-steel gas manifold system, and a data logging and control.

106 These flasks (0.7 L each) are pressurized to obtain 2.2 L of sample air from each target altitude. Air samples are then

107 shipped back to NOAA/ESRL for carefully calibrated and quality-controlled measurements. Carbon dioxide is

108 measured using a nondispersive infrared analyzer. Long-term measurements at ~15 sites are carried out using light

109 aircraft that can reach 8.5 km. Air samples are collected mostly during late morning to early afternoon, when the air

110 mass within the planetary boundary layer (PBL) is generally well mixed, and CO_2 enhancement near the ground

111 from plant respiration during the night has been mixed throughout the boundary layer. Normally, the aircraft follows

112 a pre-decided route such that most samples are collected within 0.1° of the site location. The sampling frequency

113 varies from site to site, currently from twice a month to once every 1.5 months. For more sampling details, quality

114 control discussions, and an evaluation of the sampling frequency, please refer to Sweeney et al. (2015). More

115 information on the aircraft sites can be found at http://www.esrl.noaa.gov/gmd/ccgg/aircraft/. We estimate the

116 uncertainty of individual measurements of CO_2 in flask air (68% confidence level) at 0.08 ppm. However, we have

117 seen evidence of positive biases for samples collected using older flasks that may contain contaminants.   Andrews

118 et al. (2014) reported biases that increased from <0.1 ppm in 2008 to an average offset in 2013 of 0.36 ppm. The

119 aircraft sampling protocol was modified starting in August 2014 to mitigate this bias. For samples collected prior the

120 protocol change, laboratory tests showed that new/clean flasks have zero bias, but some older/dirty flasks could have

121 biases of > 1 ppm. This bias is not consistent among individual flasks and increasing over time (Andrews et al.,

122 2014), the potential bias is hard to quantify for measurements before August 2014. Thus, the high bias is not

123 corrected in our study. More recently, low bias has been found in PFP measurements when the ambient humidity is

124 high, based on comparisons of PFP measurements with data from in-situ analyzers at tall towers. We are working to

125 understand and quantify this bias, and for this study we have derived a preliminary correction factor, which shows a

126 linear trend with -1.4 ppm CO_2 offset per 1% above 1.7% of ambient water (mole fraction relative to whole air)

127 content. Only ~ 4% of total aircraft measurements or ~ 12% of those below 2 km are impacted by humidity higher

128 than 1.7%, for which we have applied corrections before data analysis. The mean correction applied is 0.53 ± 0.4 (1

129 σ) ppm for the impacted data.

130   The NOAA tall tower network measures CO_2 and other trace gases within the continental boundary layer.

131 Continuous in-situ measurements are conducted using nondispersive infrared (NDIR) absorption sensors and cavity

132 ring-down analyzers. The long-term stability of these systems is typically better than 0.1 ppm for CO_2 (Andrews et

133 al., 2014). Most tall tower sites have more than one air intake height. In this study, continuous in-situ measurements

134 from the highest intake are used to minimize potential influences from local sources. More information concerning

135 the tower sites can be found at http://www.esrl.noaa.gov/gmd/ccgg/insitu/. For the column XCO_2 calculation, tower

136 data only from 10:00-17:00 local standard time (LST) on flight days are averaged to one data point per day, as a

137 complement to vertical profiles within the PBL.

138 **2.2 Site description**

139 We analyze data from 19 aircraft sites and 6 tall tower sites during 2004 to 2014 (see Table S1 for a summary of site

140 conditions). After considering the geographic distribution of these sites in North America, we group them into eight

141 regions for spatial comparisons (Fig. 1). The northern west (NW) and southern west (SW) regions represent the

142 inflow area in the west coast of US, directly downwind of the Pacific Ocean at both higher elevations. The northern

143 mid-continent (NM) region represents the boreal forest and agriculture region in north-central North America. The

144 mid-continent (MC) region represents a dry landscape due to its high elevation (above 1.5 km on average) and semi-
145 arid climate. The mid-west (MW) region is strongly influenced by agriculture and temperate forest. The southern
146 mid-continent (SM) represents the south-central humid temperate region, with inflow from the Gulf of Mexico
147 during summer. The northeast (NE) region represents the temperate forest in north-east coast of U.S., which is
148 mostly downwind of regions to the west above the PBL, and downwind of its south-west regions within the PBL.
149 The southeast (SE) region represents the warm temperate region in the south-east coast of U.S.

150
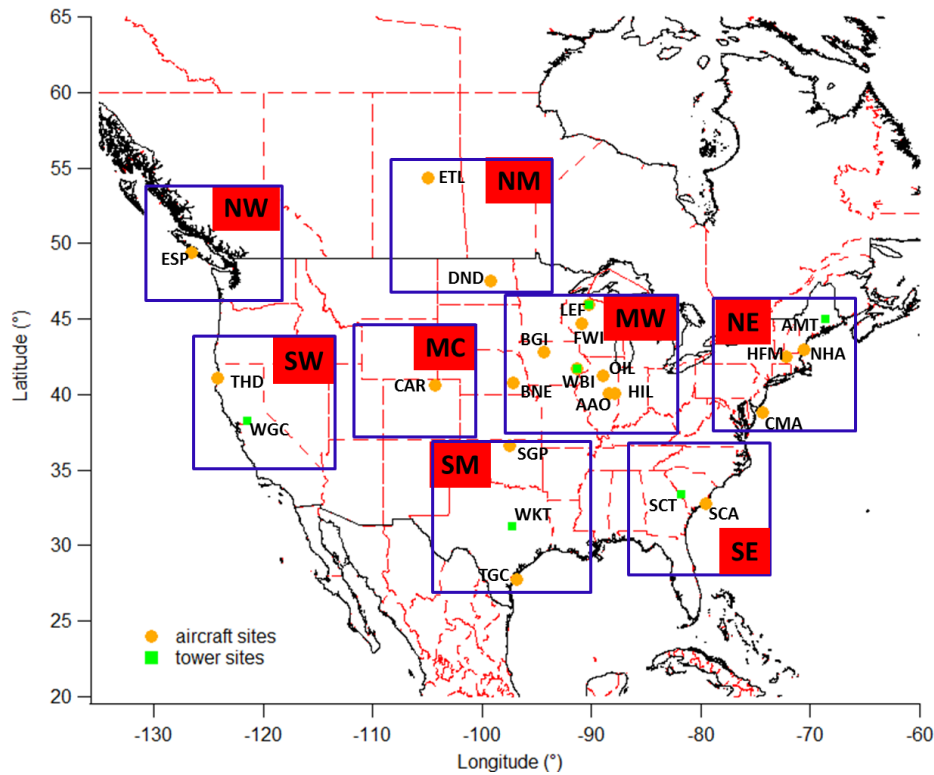
151
152 **Fig. 1.** Aircraft, tall tower, and high elevation/tower sites in the NOAA GGGRN. The eight boxes define regions
153 that are further discussed for spatial pattern comparison.

154 **2.3 Smoothing of the reference data and column XCO$_2$ calculation**

155 We use Mauna Loa Observatory (MLO) as a reference site. MLO is located at 19.536°N, 155.576°W, and 3397 m
156 above sea level. Carbon dioxide measurements from this site are widely used to represent background CO$_2$ in the
157 Northern Hemisphere. For our study, a function consisting of a quadratic polynomial and four harmonics is fitted to
158 the MLO data, adopted from the method described by Thoning et al. (1989). Residuals of the data from this function
159 are smoothed by a low-pass filter with full-width at half-maximum in the time domain of 1.1 years. The smoothed
160 residuals are then added back to the polynomial part of the function to produce the long-term deseasonalized trend.
161 This trend (see Fig. 3) is subtracted from all aircraft and tall tower measurements. Also, the CarbonTracker results
162 presented in this study are the differences relative to observed MLO deseasonalized trend. We use 'Δ' to represent
163 detrended data in the following text and figures. The choice of reference site is not important for this study, since

 we focus on examining the relative seasonal patterns of the detrended spatial and vertical distributions of CO_2

165 instead of the total changes in CO_2 abundance attributed to global surface fluxes.

166

Oct. 11, 2012        Oct. 23, 2012
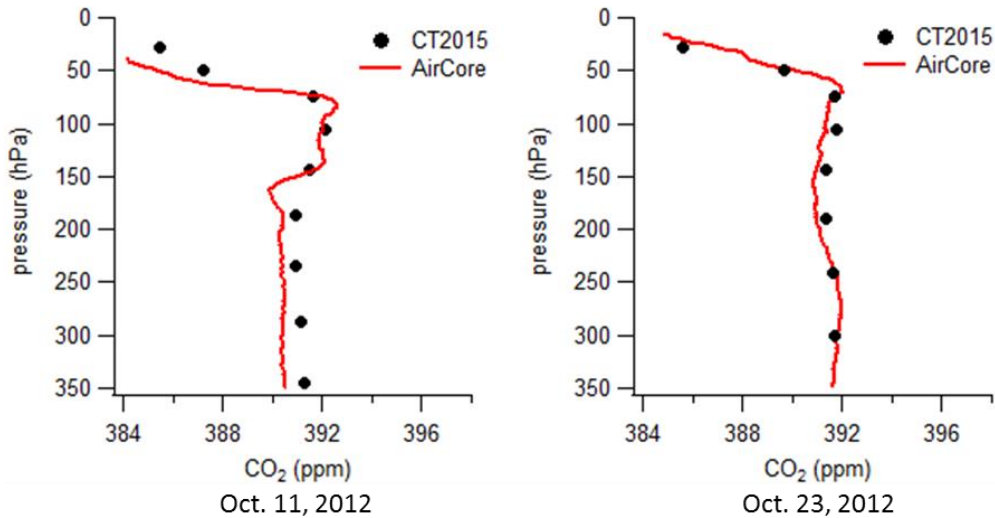
167

168 **Fig. 2**. Carbon Tracker (CT2015) simulations compared with AirCore in-situ measurements in upper atmosphere.

169 AirCore profiles in the left and right panels are sampled near CAR and SGP, respectively.

170

171   We calculate partial column average CO_2 dry mole fraction using tall tower and aircraft data, and the total

172 column by adding simulations of high altitude CO_2 (above 330 hPa, ~ 8 km above sea level) from CarbonTracker.

173 Since geometric height from the onboard Global Positioning System (GPS) (after 2006) or inferred from the aircraft

174 altimeter or pressure altitude is archived with each aircraft measurement, we first convert geometric height (in

175 meter) to pressure (in hPa) for the pressure-weighted column XCO_2 calculation. This conversion uses geopotential

176 data from NOAA/NCEP North American Regional Reanalysis (NARR) (Mesinger et. al, 2004), available at

177 https://www.esrl.noaa.gov/psd/data/gridded/data.narr.html, in which the geopotential is a function of latitude,

178 longitude, pressure altitude and time. We interpolate the geopotential field vertically to retrieve pressure, and then

179 calculate dry pressure by incorporating specific humidity data from NARR. Eventually we use a trapezoidal method

180 to integrate over detrended vertical profiles for dry-pressure-weighted column averages. For the long-term averaged

181 column ΔXCO_2 calculation, a long-term mean vertical profile is first constructed for each month by combining 11-

182 year detrended data together and then average data in each 40 hPa vertical bin. To look at the long-term averaged

183 total column ΔXCO_2 from individual aircraft sites, we combine aircraft data with upper-layer CT2015 simulations.

184   The NOAA CarbonTracker model assimilates CO_2 measurements from surface sampling networks and tall

185 towers to generate global 3D fields of atmospheric CO_2 mole fraction. The Carbon Tracker model has evolved

186 significantly since Peters et al. (2007). A detailed description of this model is provided in documents available at

187 http://carbontracker.noaa.gov. Our study utilizes CarbonTracker results from the 2015 release (CT2015), publicly

188 accessible at ftp://aftp.cmdl.noaa.gov/products/carbontracker/co2/CT2015/molefractions/. This version provides

189 CO_2 mole fraction over North America with $1° \times 1°$ spatial and 3 hour temporal resolutions, which are analyzed in

190   Sect. 3.2 and 3.3. Total column CO_2 calculated from CT2015 global data with $3° \times 2°$ spatial resolution is also

191   presented in the supporting information (SI). We have evaluated the performance of CarbonTracker in upper

192   atmosphere (330 to 0 hPa) by comparing its simulations with in-situ measurements from 9 AirCore profiles (Karion

193   et al., 2010) sampled in 2012-2014. AirCore is a ~150 m stainless steel tube that utilizes changes in ambient

194   pressure for passive sampling of the vertical profile. The tube is carried to high altitude by balloon and it collects a

195   continuous sample as it descends. It is then measured by an analyzer after it is recovered. More information about

196   AirCore system can also be found at https://www.esrl.noaa.gov/gmd/ccgg/aircore/. All 9 AirCore profiles are taken

197   near SGP and CAR sites. Figure 2 shows examples of AirCore profiles compared with CT2015 in the upper

198   atmosphere, which demonstrates good agreement. We also compare partial column (330 to 0 hPa) averages from the

199   9 AirCore profiles and CT2015. Results from CT2015 agree generally well with AirCore, with difference ranging

200   from 0.03 to 1.22 ppm (mean value equals 0.66 ppm), which suggests that CT2015 may have a high bias that could

201   contribute to $0.66 \times 1/3 = 0.22$ ppm overestimate on average to the total column average. However, AirCore is in the

202   process of rigorous evaluation, the differences between AirCore and CT2015 are not well characterized yet since we

203   only have a limited amount of AirCore data. It is unclear whether the potential bias of CT2015 in this partial column

204   is dependent on time or sampling location. Adding a constant bias correction to all regions will not change the

205   spatial gradients that we focus on in this study. Thus no correction is applied when using CT2015 simulations to

206   represent the upper 1/3 of the total column. For uncertainty estimates, we use a "bootstrap'

207   method that uses random resampling of individual vertical profiles with restitution (low bias, high humidity was

208   corrected), with 100 Monte Carlo runs for each column average calculation. Uncertainty is then defined as one

209   standard deviation of the 100 Monte Carlo results.

210   **3 Results and Discussions**

211   **3.1 Seasonal patterns and spatial gradients**

212   Typically one aircraft profile contains measurements at 12 different altitudes. Column ΔXCO_2 can be computed for

213   each profile using the method described in Sect. 2.3 (Fig. S1). Our aircraft and CT2015 based column CO_2 at SGP

214   and LEF sites shows reasonable agreements with TCCON data retrieved at Lamont and Park Falls site

215   (Washenfelder et al., 2006; Wunch et al, 2009, 2011), respectively (Fig. S2). Figure 3 shows aircraft (at all altitudes)

216   and tower data (daily averages for 10:00-17:00 LST data) from all sites used in this study. Aircraft data above 2 km

217   exhibit much smaller seasonal variations than the full dataset, because the variations are mainly driven by CO_2

218   sources and sinks near Earth's surface. CO_2 mole fraction is enhanced in the shallow wintertime PBL primarily due

219   to reduced plant photosynthesis and ecosystem respiration combined with slightly increased fossil fuel emissions.

220   During summer the PBL is deeper, and depletions within the PBL are due to strong terrestrial uptake that dominates

221   over emissions especially during June through August. During summer of 2010 to 2012, CO_2 from aircraft

222   measurements appears higher than other years in Fig.3; however, similar characteristics are not present in tower

223   data. This apparent difference is due to a decrease in sampling frequency at several aircraft sites that resulted in an

224 aliased picture of the full summer signals. Since we focus on climatological mean of 11 years of data in our study,

225 this influence is eliminated by combining 11 years of data together into one "average year".

226
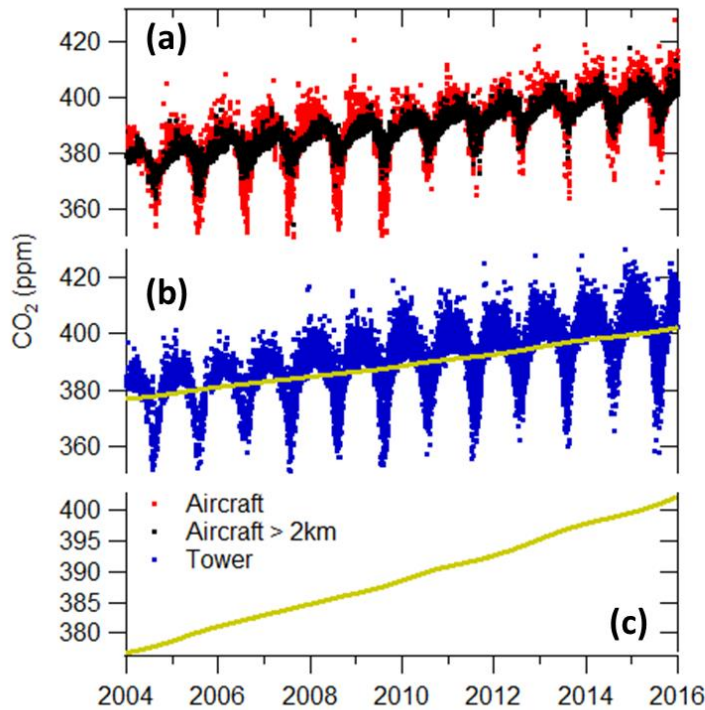
Fig. 3. CO_2 observations from aircraft (a) and towers (b). The yellow line in (b) illustrates the deseasonalized trend

228 at Mauna Loa (MLO), same as in (c), in which y-axis is expanded.

229

230   To investigate the contributions of different altitudes to spatial gradients between regions, we divided all

231 measurement data into three layers according to their sampling altitudes: below 2 km, 2 - 5km, and 5 - 8.5 km masl

232 (Fig. 4). Smooth seasonal curves are attained from fitting data with four harmonics using the method described by

233 Thoning et al. (1989). The peak-to-valley amplitudes of the seasonal cycles below 2 km are the largest among the

234 three layers for most regions, with a minimum of 10.3 ppm in SM and a maximum of 25.0 ppm in MW. The

235 seasonal variation amplitudes decrease to 7.7-11.5 ppm in the 2 - 5 km layer, and further decrease to 7.2-10.0 ppm in

236 the 5 - 8.5 km layer. We also observe that the seasonal cycle drawdown occurs later in the layers above 2 km (see

237 Fig. S3, which provides similar information as Fig. 4, but seasonal curves from different vertical layers are grouped

238 by regions to facilitate comparisons of the phases of seasonal cycles). The seasonal CO_2 drawdown below 2 km is

239 mainly influenced by terrestrial photosynthesis and gradients are due to local to regional fluxes, with an earlier onset

240 of drawdown in southern regions than in northern regions. The seasonal cycle aloft is damped and lagged compared

241 to the PBL, with influences from throughout the Northern Hemisphere and with spatial gradients likely driven by

242 large-scale transport. The NW, SW, SM, and SE inflow regions have significant delays of more than one month in

243 the 2 - 5 km layer compared with the surface layer, which is likely due to the delayed phase of the seasonal cycle in

244 well-mixed air coming from the oceans. Vertical homogeneity of air over ocean was observed during the HIAPER
245 Pole-to-Pole Observations (HIPPO) aircraft campaign (Wofsy et al., 2011; Frankenberg et al., 2016). As air masses
246 are transported further inland, we observe reduced discrepancies of the timing of CO_2 drawdown between surface
247 and upper layer air (2-5 km), which may be associated with the increased influence of the land surface in the mid-
248 troposphere due to strong convection over land. CO_2 drawdown in the 5 - 8.5 km layers also occurs later than in the
249 2 - 5 km layers in most regions; however, differences between these two layers are small. The declining amplitude
250 and delayed phase of the seasonal cycle with altitude have been noted often (e.g., Tanaka et al., 1983; Ramonet et
251 al., 2002; Gerbig et al., 2003, Sweeney et al. 2015). It demonstrates that there is lot of important information in the
252 vertical profile that is diminished in observations of the total column.

253   We find that the largest horizontal spatial gradients between regions occur below 2 km during summer time
254 (Fig. 4), with a maximum difference of ~15.5 ppm between MW and SM. SM and SW exhibit less pronounced
255 seasonal cycles, which is likely associated with air masses from the Gulf of Mexico and the Pacific Ocean,
256 respectively, whereas MW exhibits a deep summer drawdown (amplitude in seasonal cycles) partially as a result of
257 strong regional forest and crop uptake. Crevoisier et al. (2010) estimated the surface flux over North America using
258 vertical CO_2 measurements and average wind vectors, and reported that annually averaged land carbon fluxes in the
259 western (including SW region) and southern regions (including SM region) were neutral. The SE region also
260 demonstrates a less pronounced seasonal cycle with higher summertime levels compared with other northern
261 regions, which may be due to the sea-breeze influence in summer within PBL. In wintertime, CO_2 levels in NE and
262 MW are higher than in other regions, which result from regional fossil fuel and terrestrial biogenic emissions
263 combined with transport from the west and south.

264   Higher altitude data (above 2 km) exhibit only small spatial gradients. In the 2 - 5 km layer, the largest gradient
265 is 4 ppm in summer (Fig. 4b). It further decreases to less than 3 ppm in the 5 - 8.5 km layer (Fig. 4c). Figure 4d
266 shows modeled CO_2 mole fractions from CT2015 for the upper troposphere and above (330 hPa to 0 hPa), which are
267 used to fill in above the aircraft profiles for calculation of total column ΔXCO_2. Spatial gradients in this layer are
268 less than 0.5 ppm, suggesting that the top third of the total column has little contribution to the spatial gradients of
269 the total column.
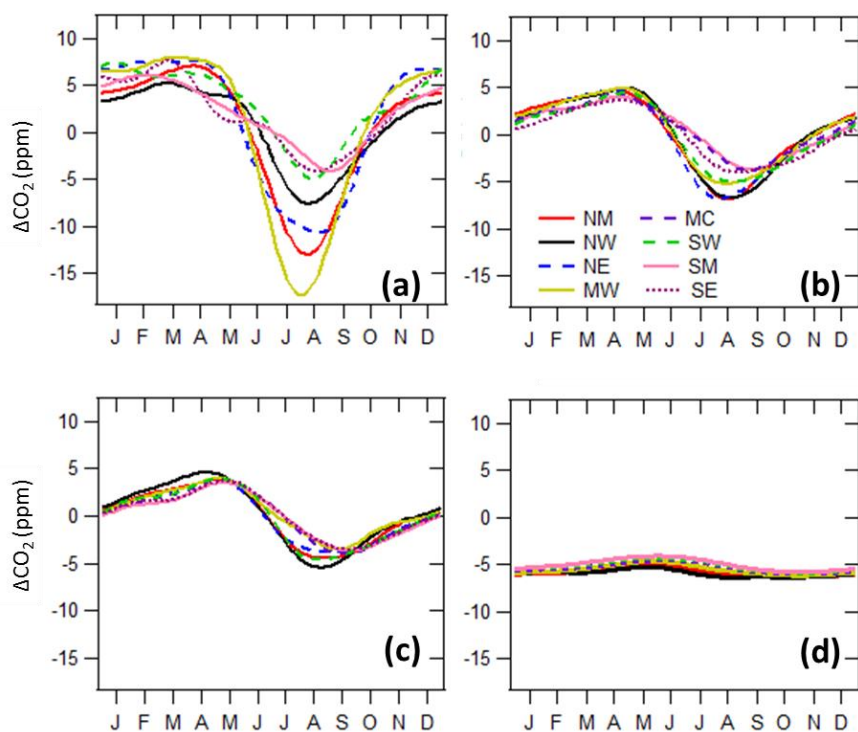
Fig. 4. Multi-year (2004-2014) average smooth seasonal curves of CO_2 relative to the long-term de-seasonalized trend at Mauna Loa for different vertical layers: (a). Aircraft and tower data under 2 km, MC is not presented because only limited data were available due to high surface elevations (>1.5 km on average) in this region; (b). Aircraft data from 2 - 5 km; (c). Aircraft data from 5 - 8.5 km; (d). CT2015 model results for layers above 330 hPa (~8.5 km) to 0 hPa (~80 km).

3.2 Long-term mean vertical profiles

To investigate the mean spatial gradients, we first calculate the long-term mean monthly vertical profiles as described in Sect. 2.3. In addition, each tower serves as one additional layer in the mean profile. The long-term mean tower data generally fit well in the vertical profiles from measurements of aircraft samples (Fig. 5 and Fig. 6), suggesting that the biases described in Sect. 2.1 above do not significantly affect the long-term mean. To attain profiles of the entire atmospheric column, upper layers (330 to 0 hPa) are filled in by CT2015, and the lowest data point of the measured profile is extended to ground level, defined by the mean surface elevation in that region.

Figure 5 presents two examples of long term mean profiles with data variability, which is the one standard deviation for each 40 hPa bin of aircraft data or for all flight-day tower data. Variability as large as 20 ppm is seen within the PBL in the MW region in summer, which is due to strong and heterogeneous surface vegetation uptake and ecosystem respiration combined with day-to-day changes in wind direction. All long-term mean monthly vertical profiles are presented in Fig. 6, which shows the mean temporal and vertical variability of CO_2 in each season, and further demonstrates the vertical propagation of seasonal CO_2 due to changes of surface flux. In

289 wintertime, monotonic decrease of CO_2 with altitude can be observed from all regions, in which high PBL CO_2 is

290 mainly driven by surface emissions and reduced vertical mixing (Denning et al., 1998; Stephens et al., 2007).

291 Surface CO_2 decreases dramatically in the growing season in those regions influenced by high plant activity, such as

292 NM and MW regions. For the summer vertical profiles in NE and SE region (east coast of the U.S.), the CO_2 mixing

293 ratio is elevated in the layer under 900 hPa followed by significant decreases in upper layers until 750 hPa, and then

294 increases with altitude until tropopause (Fig. 6). This is likely a result of sea breeze influence. Lower-troposphere air

295 from the sea, lacking terrestrial uptake of CO_2, typically has higher CO_2 in summer compared with inland air.

296 Polluted air previously advected offshore can be brought back along with sea breeze. Without significant vertical

297 mixing over the marine surface, high levels of pollutants remain in those air masses. The convergence of sea breeze

298 with prevailing wind moving offshore may create a period with a stalled frontal structure that can aggregate air

299 pollutants (Banta et al., 2005). The convective internal boundary layer structure of the sea breeze system can

300 significantly reduce mixing height (Miller et al., 2003), and also induces higher CO_2 levels. When the sea breeze is

301 not dominant, air advected from southwest and west (the land) can also bring in polluted air with high CO_2 since this

302 region is downwind of continental U.S. emissions (Miller et al., 2012).
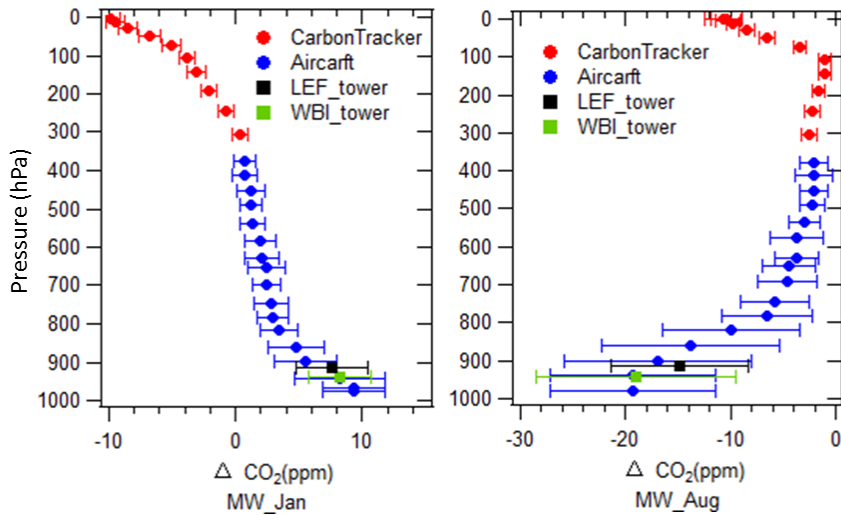
303

304 **Fig. 5**. Long-term mean (2004-2014) average vertical profiles in January (left panel) and August (right panel) in

305 region MW. Error bar shows one standard deviation.
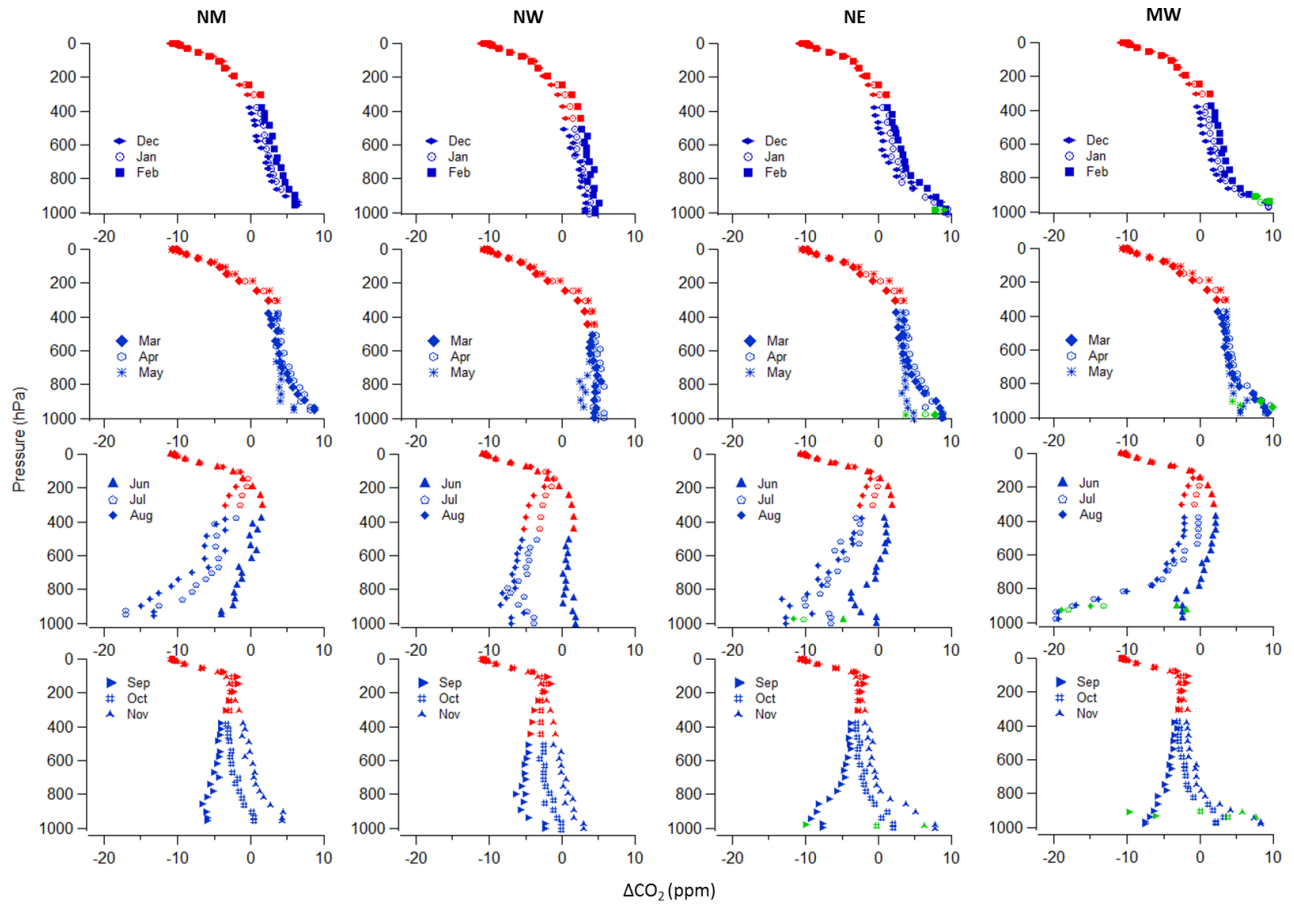
306

307 **Fig. 6a**. Long-term mean (2004-2014) monthly vertical profiles in NM, NW, NE, MW (by column, from left to

308 right). Blue points were calculated from observations, red points were calculated from CT2015, and green points

309 were calculated from tower data.
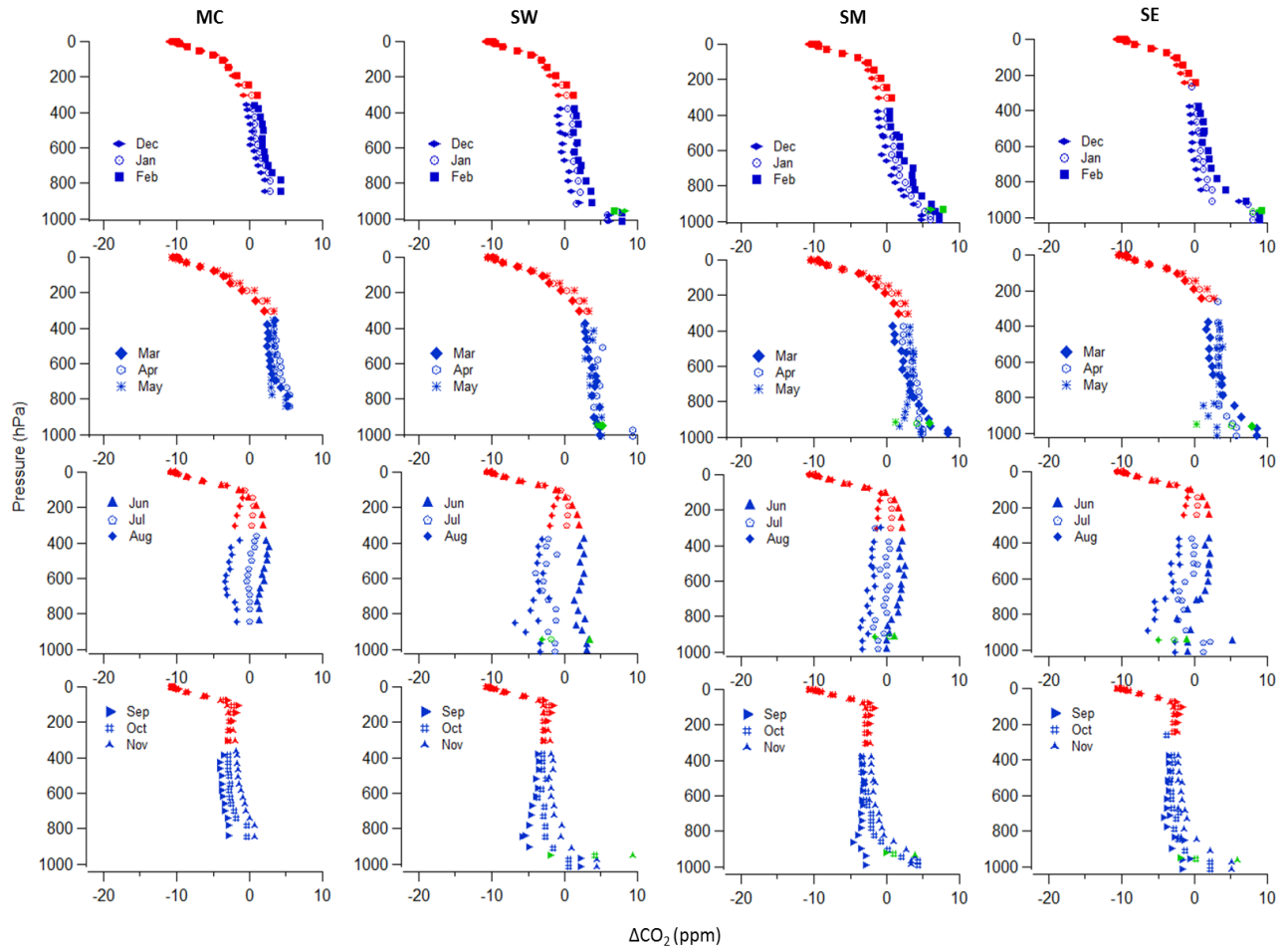
310

311 **Fig. 6b**. Long-term mean (2004-2014) monthly vertical profiles in MC, SW, SM, SE (by column, from left to right).

312 Blue points were calculated from observations, red points were calculated from CT2015, and green points were

313 calculated from tower data.

314

3.3 Partial column ΔXCO₂ and total column ΔXCO₂

Seasonal variations of monthly averaged partial column ΔXCO_2 (below 330 hPa) demonstrate maximum values in April and minimum values in August or September (Fig. 7a). The largest amplitude appears in NM, with peak-to-valley difference up to 13.5 ppm. SW, SM, SE, and MC have similar amplitudes of 7-8 ppm, smaller than the other three regions. To evaluate the performance of CT2015 on column ΔXCO_2, CT2015 results are sampled to match the latitude, longitude, altitude and time of actual measurements. Note that aircraft profiles are not assimilated in CT2015, so aircraft data are independent of the CT2015 data assimilation. Figure 7b shows monthly partial columns of ΔXCO_2 calculated from CT2015, which demonstrate good agreement with results from measurements. Only small seasonal biases exist in CT2015, with high bias occurring mostly in spring and early summer and low bias in September and October (Fig. S4). The overall differences of monthly partial column ΔXCO_2 (CT2015 - measurements) mainly fall in the range of -0.64 ppm (5th percentile) to 0.84 ppm (95th percentile) with a mean difference of 0.13 ppm. These differences are of similar magnitude to the uncertainties of partial column ΔXCO_2 calculated from the measurements (Fig. S5). It is clear that CT2015 captures the long-term mean variations of both phase and amplitude of partial column XCO_2 reasonably well when compared with well-calibrated measurements across North America.
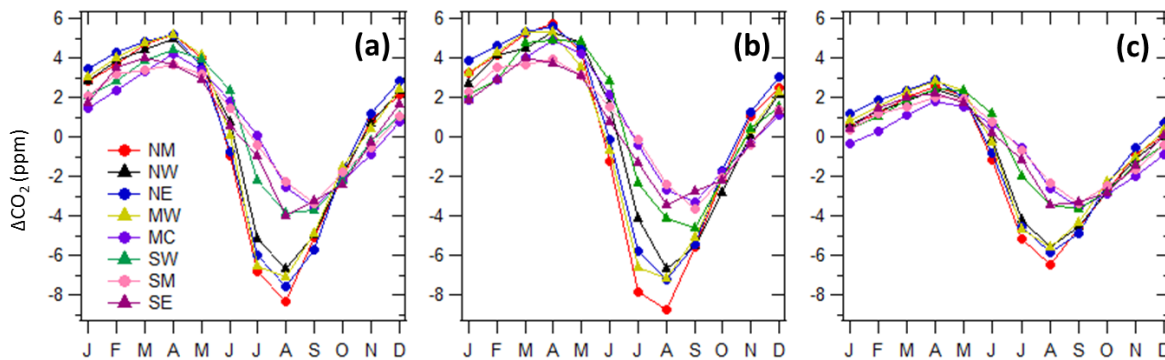
Fig. 7. (a). Partial column ΔXCO_2 calculated from aircraft and tower data; (b). Partial column ΔXCO_2 calculated from CT2015; (c). Total column ΔXCO_2 calculated from aircraft and tower data and including the top layer data from CT2015.

Total column ΔXCO_2 is presented in Fig. 7c. In regions NW, NM, NE, and MW, seasonal variations of total column ΔXCO_2 are very similar in both phase and amplitude (8-9 ppm peak to valley). For SW, SM, SE, and MC, amplitudes are ~5.5 ppm. The smallest spatial gradients occur during May and October, which result in maximum differences among all regions of only 0.9 and 0.7 ppm, respectively. The largest spatial gradients occur during June, July and August, which result in maximum differences of 2.4, 4.5, and 4.1 ppm, respectively. It is interesting that the deepest seasonal drawdown is seen in region NM, not in region MW that encompasses the very intensive

342   agricultural activities in the U.S. mid-west, which suggest the possibility of strong upwind influence in the NM

343   region. Transported signals have significant influences on total column CO_2. The summer total column ΔXCO_2,

344   represented by the June to August average from CT2015, has a magnitude that is similar to observations with

345   differences no more than 1 ppm (Fig. 8). Based on the seasonal patterns of total column ΔXCO_2 (Fig. 7c) and the

346   summer column ΔXCO_2 (Fig. 8), we can separate the eight regions into two groups. The group with NW, NM, NE,

347   and MW, has ~3 ppm stronger drawdown (larger amplitude) than the group with SW, SM, SE, and MC. For winter

348   total column ΔXCO_2 (December to February average), the maximum spatial difference is only 1.6 ppm, with the

349   highest total column ΔXCO_2 of 1.2 ppm in NE and the lowest value of -0.3 ppm in MC.

350
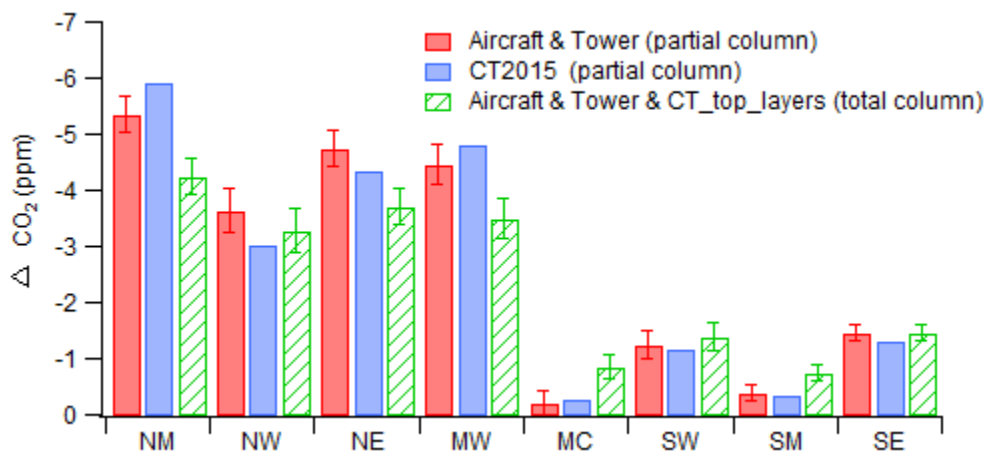
351

352   **Fig. 8**. Long-term mean (2004-2014) June to August partial and total column ΔXCO_2. Error bars represent one

353   standard deviation from the bootstrap uncertainty calculation (see Sect. 2.3).

354

355   **3.4 Influence of large scale circulation**

356   Figure 9 shows long-term mean summer column ΔXCO_2 calculated from CT2015, together with full column

357   ΔXCO_2 from individual aircraft sites. Note that some aircraft sites have less than 11 years of data that CT2015

358   shows in Fig. 9, only aircraft sites with more than 6 years of data are presented, the actual values are provided in

359   Table S2. The fact that total column ΔXCO_2 from CT2015 agrees well with aircraft sites supports the performance

360   of CT2015 on a long-term average basis. The observations show a similar summer spatial pattern, with lower

361   column ΔXCO_2 in the north and northeast regions and higher column ΔXCO_2 in the south and southwest regions

362   (Fig. 9a). Scattered hot spots of high column ΔXCO_2 associated with surface emissions from megacities, or cold

363   spots associated with strong local uptake, are not or just barely visible in the long-term average column ΔXCO_2 map

364   at 1°x1° resolution. Instead, the wave-like pattern of column ΔXCO_2 over North America reflects the average large

365   scale circulation. To support our hypothesis on the influence of large scale circulation, we analyze the long term

366   mean wind pattern over North America. We can see that air masses from northwest of the continent bring in low

367   average column ΔXCO_2, while air masses from the south (mainly the subtropical Pacific Ocean and the Gulf of

368   Mexico) bring in high column ΔXCO_2 (Fig. 9b). The zonal gradients over the continent, especially north of 40° N,

369   also reflect long-term average wind patterns; southwest wind corresponds to higher column ΔXCO_2 over the western

370   part of the continent until the wind direction shifts to west-northwest over the eastern part of the continent. This

371   wind pattern matches well with the geographic division of the over/under -3 ppm areas colored in green/blue in the

372   column ΔXCO_2 map (Fig. 9b). Figure 9c and 9d shows partial column averages for free troposphere (800-330 hPa)

373   and lower troposphere (below 800 hPa), respectively. The free troposphere spatial gradient also demonstrates a

374   wave-like pattern. A previous study on the total column CO_2 from ground based Total Carbon Column Observation

375   Network (TCCON) found strong correlation between the mid-latitude column CO_2 and synoptic-scale variation of

376   potential temperature (θ, at 700 hPa), a dynamic tracer for adiabatic air transport (Keppel-Aleks et al., 2012). Thus

377   they also propose that the variations in column CO_2 are mainly driven by large-scale flux and transport. Analysis of

378   the interannual variability of the seasonal cycle amplitudes of column CO_2 in North Hemisphere has also found

379   significant contribution of large-scale circulations to the north-south gradient (Wunch et al., 2013).

380   The strong drawdown over northeast North America in summer is a consequence of long-range transport of low

381   CO_2 from northeast Eurasia, in addition to regional terrestrial uptake. Sweeney et al. (2015) notes well-mixed

382   vertical profiles (up to 8 km) of CO_2, CO, CH_4, N_2O, and SF_6 from THD, ESP and PFA (Poker Flat, Alaska; 65.07°,

383   -147.29°) sites and suggests that air coming across the Pacific was strongly influenced by Asian surface fluxes

384   before being vertically homogenized as it passed over the Pacific Ocean. This well-mixed air forms an important

385   boundary condition in the column CO_2 of air coming into the North American continent. This was best illustrated at

386   sites like PFA where the summertime minimum in CO_2 significantly preceded maximum ecosystem uptake of CO_2,

387   implying significant influence of transported air from lower latitude regions from Asia. We further conduct an

388   experiment using Carbon Tracker to investigate the importance of this effect. A control run and a "masked run" are

389   conducted for 2010-2012, in which the Eurasian boreal flux is turned on/off. The MLO CO_2 trend from each model

390   scenario is used as reference background and thus removed before total column ΔXCO_2 calculation. Figure 10 shows

391   the results for 2012 summer, which is an average summer when compared with the 2004-2014 mean pattern (Fig. 9

392   and Fig. 11). The maximum north-south difference reduces to ~2.5 ppm after we turn off the Eurasian boreal flux,

393   compared with ~5 ppm from the control run. In both control and masked scenarios, the free troposphere partial

394   ΔXCO_2 demonstrates similar spatial patterns as for total column ΔXCO_2 (Fig. S6). This result combined with results

395   from Sweeney et al. (2015) demonstrates that the transport of low CO_2 resulting from large summertime Eurasian

396   boreal uptake has a large contribution on the overall summer total column CO_2 decrease in North America.

397

398
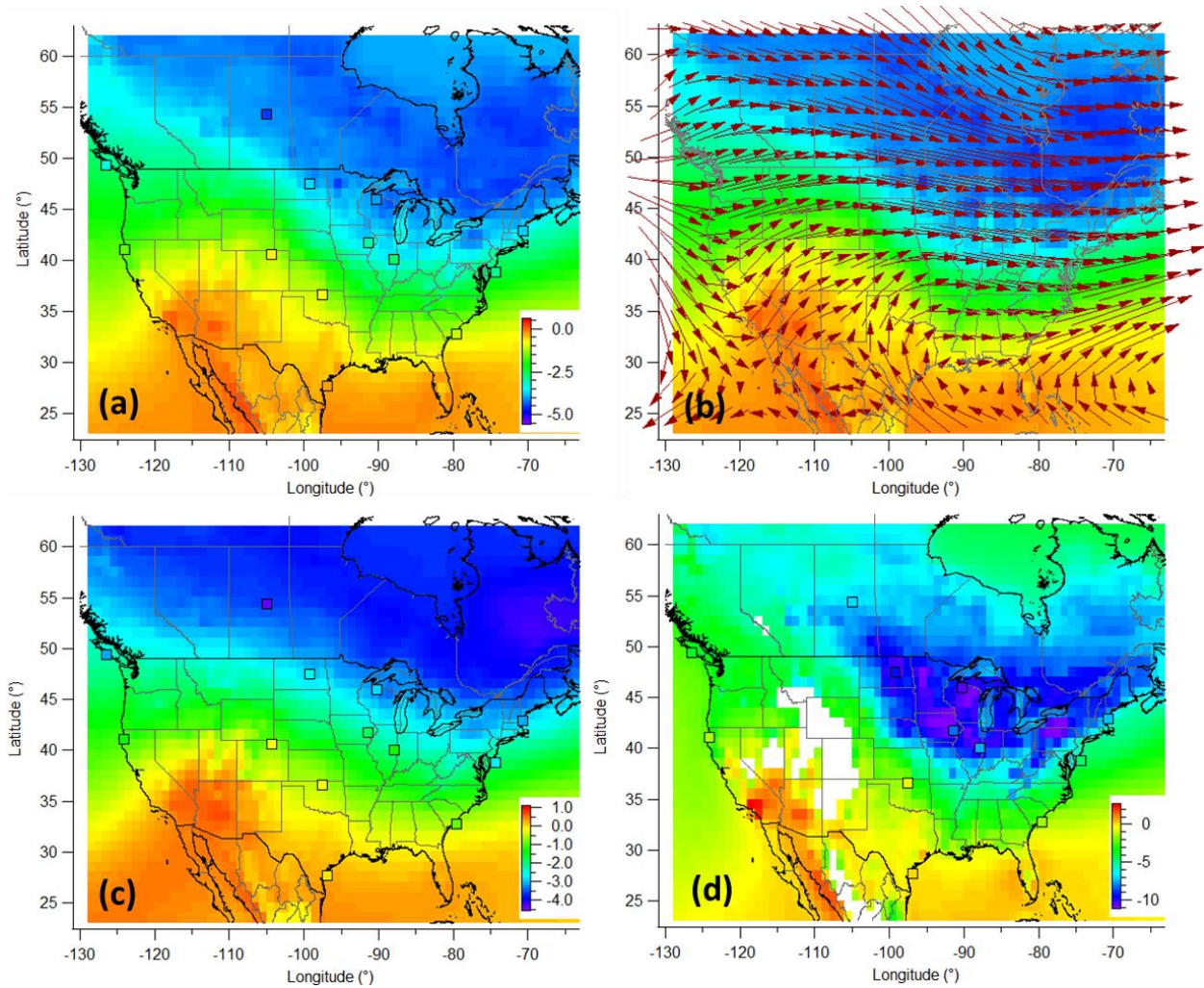
Fig. 9. Long-term mean (2004-2014) June-August total column ΔXCO_2 from CT2015 in $1° \times 1°$ spatial resolution with total column ΔXCO_2 for 13 individual aircraft sites in squares (a), and CT2015 column ΔXCO_2 overlaid with pressure-weighted (1000 hPa to 500 hPa) mean wind vectors for the same period (b). (c) and (d) are similar as (a), except for free troposphere (800 to 330 hPa) and lower troposphere (below 800 hPa), respectively. Note the different color scales.

406
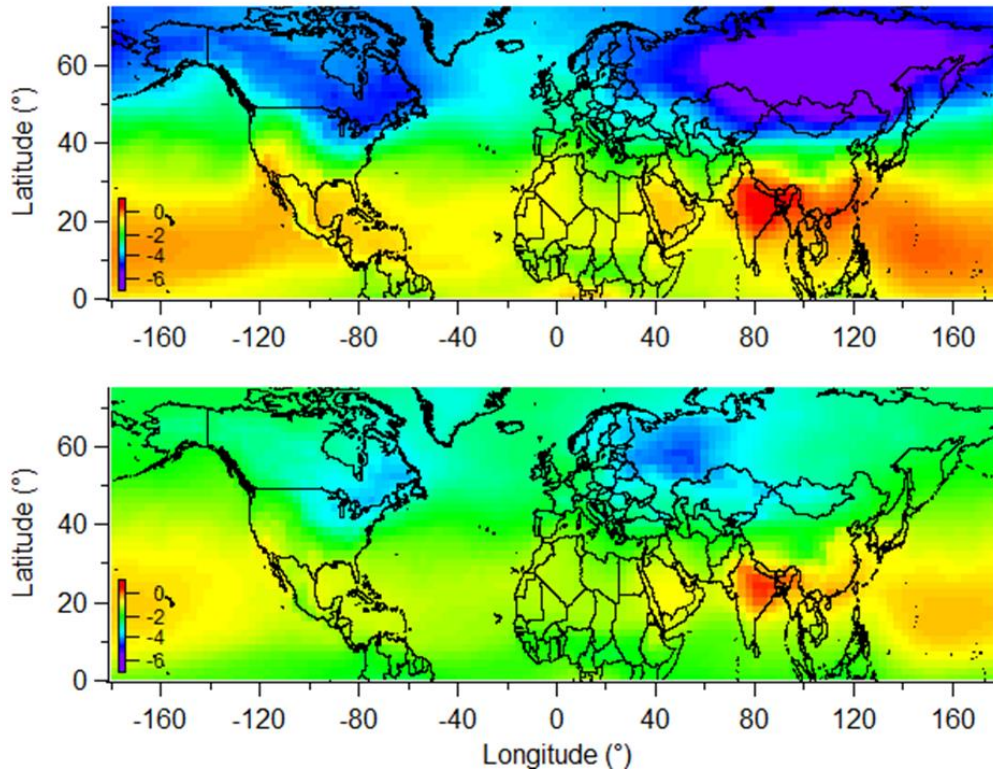
Fig. 10. Total column ΔXCO_2 from Carbon Tracker control (top panel) and masked (bottom panel, Eurasian boreal flux is masked) runs for 2012 June-August ($3° \times 2°$ spatial resolution). MLO trend from each individual scenario is removed before the ΔXCO_2 calculation. Same color scale is used as in Fig. 9a. Partial column ΔXCO_2 patterns for free troposphere (800 to 330 hPa) and lower troposphere (below 800 hPa) are provided in SI.

3.5 A comparison with apparent gradients over Europe

Figure 11 shows the climatological June - August mean modeled global column ΔXCO_2 map in $3° \times 2°$ spatial resolution, which presents smooth wave-like patterns. Reuter et al. (2014) use SCIAMACHY and GOSAT satellite retrievals of column CO_2 and inverse modelling to infer a very large net CO_2 uptake flux over European region. Column ΔXCO_2 from CT2015 (Fig. 11) exhibits a drastically different summer spatial pattern over Europe compared with the eight year mean (2003-2010) June through August satellite retrievals presented by Reuter et al. (2014, their Fig. 2a). The spatial gradient from CT2015 results in a maximum 3-4 ppm difference and a gradual pattern, instead of as much as 6 ppm from satellite retrievals. There is no sign of XCO_2 hot spots from surface emissions or removals in the CT2015 spatial pattern over Europe (Fig. 11), in contrast to several hot spots that are apparent from the 8-year averaged SCIAMACHY satellite retrievals over Ireland, U.K., Belgium, Netherland, north of Germany, and south of Sweden, and low spots over the Ukraine and Kazakhstan (Reuter et al., 2014). The SCIAMACHY retrieval pattern contradicts our understanding of the significant influence of large-scale transport on column ΔXCO_2. Although the NOAA/ESRL CT2015 (https://www.esrl.noaa.gov/gmd/ccgg/carbontracker/CT2015/) assimilates fewer observations over Europe than Carbon Tracker Europe (http://www.carbontracker.eu/), both

425   models produced similar fluxes over the European region (see both websites for detailed fluxes). The $3^o \times 2^o$ grid

426   from CT2015 is not likely responsible for a much smoother pattern for Carbon Tracker, compared with the $2^o \times 2^o$

427   grid from satellite retrievals (Reuter et al., 2014) . The North America region on the $3^0 \times 2^0$ grid in Fig. 11 shows

428   similar pattern as the $1^o \times 1^o$ grid in Fig. 9, with similar spatial difference of ~ 5 ppm. A smoother spatial

429   distribution should be expected in Europe for the long-term mean column XCO_2 (Fig. 11) due to the influences of

430   dominating west and southwest winds in summer. We have also evaluated the importance of sampling bias by

431   sampling CT2015 at the same latitude/longitude/date as by SCIAMACHY (Reuter et al., 2011). The 3-year (2005-

432   2007) mean pattern shows much smaller gradients without significant hot/cold spots at those locations as

433   SCIAMACHY (Fig. S7). Sampling bias is unlikely the main reason for the unphysical column XCO_2 spatial pattern

434   from SCIAMACHY. Since the satellite retrievals in Reuter et al. (2014) appear to show unrealistic column XCO_2

435   spatial gradients over Europe, they should not be used to derive any estimates of a European carbon sink. A recent

436   study (Feng et al., 2016) using inverse modeling suggests that satellite retrievals outside the immediate European

437   region and a small bias of only 0.5 ppm were sufficient to produce the apparent large carbon sink in the study of

438   Reuter et al. (2014). This is expected from elementary mass balance considerations as in Sec.1 above. Spatial

439   gradients are the fundamental signals to infer regional fluxes. Since spatial gradients from CT2015 are realistic,

440   boreal fluxes inferred by CT2015, which shows 0.03 ± 2.33 Pg C yr^{-1} for Europe, should be more trustworthy than

441   fluxes estimated based on unrealistic spatial pattern. However, the European carbon sink is still inconclusive; the

442   discrepancies among different methods and results are further discussed by Reuter et al. (2017). Increasing the

443   amount of highly precise observations such as the well-calibrated surface measurements and vertical profiles can

444   greatly help to estimate the carbon sink.

445

446
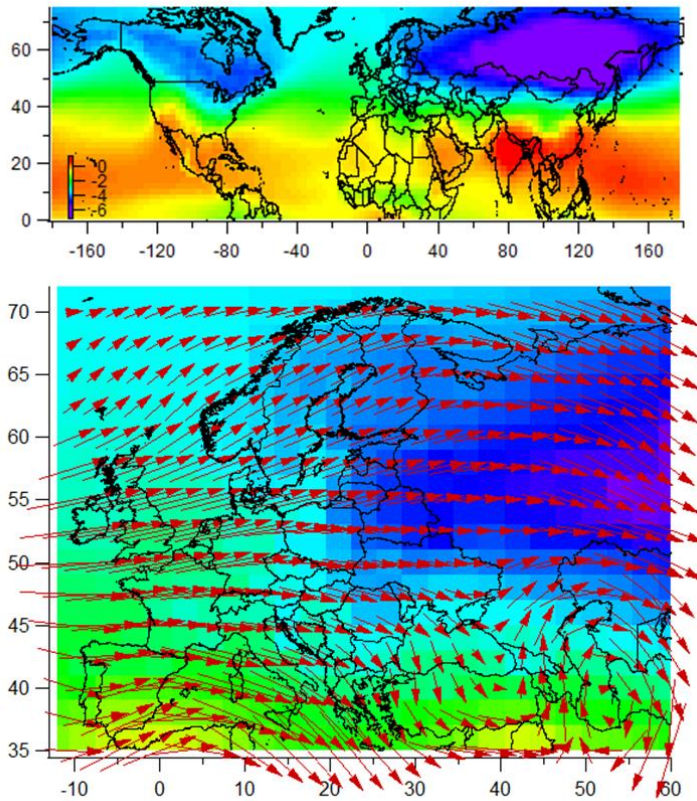
447

448   **Fig. 11**. Long-term mean (2004-2014) June - August total column ΔXCO_2 from CT2015 (top panel) in $3° \times 2°$

449   spatial resolution, and detail for Europe overlaid with pressure-weighted (1000 hPa to 500 hPa) mean wind

450   vectors for the same period (bottom panel). The color scale is the same as in Fig. 9a, which is scaled to reflect 6

451   ppm difference of XCO_2 to compare with satellite retrievals from Reuter et al. (their Fig. 2a, 2014).

452   **4 Conclusion**

453   Aircraft and tall tower measurements from the NOAA GGGRN provide detailed information describing the long-

454   term average temporal and spatial variations of CO_2 in the PBL and the free troposphere. These data provide

455   valuable constraints for evaluating model simulations and satellite retrievals. Seasonal cycle peak-to-peak

456   amplitudes of CO_2 are largest below 2 km, where those maximum values are about twice those in the vertical layers

457   above, indicating that most of the information on surface sources and sinks resides in the continental PBL. Large

458   spatial gradients of CO_2 over North America are observed below 2 km during summer (with maximum difference of

459   ~15.5 ppm between MW and SM), while higher altitude data (above 2 km) have much smaller contributions to

460   spatial gradients, with a maximum difference of 4 ppm. The spatial differences of CO_2 in the upper troposphere and

461   above (330 hPa to 0 hPa) are less than 0.5 ppm, according to CT2015. Comparison with Aircore measurements

462   shows CT2015 performs well simulating upper tropospheric and lower stratospheric patterns.

463   Our long-term mean vertical profiles show that tower data agree well with aircraft data at similar vertical levels.

464   Partial column ΔXCO_2 was calculated from the long-term mean vertical profiles. By comparing the partial column

465   ΔXCO$_2$ from measurements with those from CT2015, we verify that CT2015 captures the long-term mean patterns

466   of both phase and amplitude of partial ΔXCO$_2$.

467   Large spatial gradients of ΔXCO$_2$ only appeared in summer, during which time the north and northeast regions

468   had ~3 ppm stronger drawdowns than the south and southwest regions. Scattered hot spots of high column ΔXCO$_2$

469   associated with surface emissions from megacities, or cold spots associated with strong local uptake, are not or just

470   barely visible in the long-term average column ΔXCO$_2$. Instead, the wave-like pattern of column ΔXCO$_2$ over North

471   America matches well with the average large scale circulation. A CarbonTracker experiment to investigate the

472   impact of Eurasian long-range transport suggests that the large summer time Eurasian boreal flux alone contributes

473   about half of the north-south column ΔXCO$_2$ gradient across North America. Considering the transported signals

474   from other upwind regions, including northern Canada, we expect that the transported signals have the overall

475   largest contribution to the total column ΔXCO$_2$ spatial gradient.

476   **Author contributions**

477   Xin Lan was responsible for study design, data analysis, and manuscript writing. Pieter Tans was responsible for

478   study design, data analysis, and manuscript improvement. Colm Sweeney and Arlyn Andrews provided

479   measurement data and improved manuscript. Andrew Jacobson provided modelled data and improved manuscript.

480   Edward Dlugokencky analyzed measurements and ensured data quality, and improved manuscript. Jonathan Kofler

481   conducted tower measurements and improved manuscript. Molly Crotwell, Patricia Lang, and Sonja Wolter

482   analyzed measurements and ensured data quality. Kirk Thoning provided data smoothing method.

483   **Acknowledgements**

484   We especially thank John Mund for extracting NARR meteorological variables for our measurements. This

485   research was supported by a fellowship from the National Research Council Research Associateship Programs.

486   **References**

487   Andrews, A. E., Kofler, J. D., Trudeau, M. E., Williams, J. C., Neff, D. H., Masarie, K. A., Chao, D. Y., Kitzis, D.

488   R., Novelli, P. C., Zhao, C. L., Dlugokencky, E. J., Lang, P. M., Crotwell, M. J., Fischer, M. L., Parker, M. J.,

489   Lee, J. T., Baumann, D. D., Desai, A. R., Stanier, C. O., De Wekker, S. F. J., Wolfe, D. E., Munger, J. W. and

490   Tans, P. P.: CO2, CO, and CH4 measurements from tall towers in the NOAA Earth System Research

491   Laboratory's Global Greenhouse Gas Reference Network: instrumentation, uncertainty analysis, and

492   recommendations for future high-accuracy greenhouse gas monitoring efforts, Atmos. Meas. Tech., 7, 647-687,

493   2014.

494   Banta, R. M., Senff, C. J., Nielsen-Gammon, J., Darby, L. S., Ryerson, T. B., Alvarez, R. J., Sandberg, S. R.,

495   Williams, E. J. and Trainer, M.: A bad air day in Houston', B. Am. Meteorol. Soc., 86, 657, DOI:

496   http://dx.doi.org/10.1175/BAMS-86-5-657, 2005.

497 Biraud, S. C., Torn, M. S., Smith, J. R., Sweeney, C., Riley, W. J. and Tans, P. P.:A multi-year record of airborne
498   CO2 observations in the US Southern Great Plains, Atmos. Meas. Tech., 6, 751-763, 2013.

499 Buchwitz, M., Reuter, M., Bovensmann, H., Pillai, D., Heymann, J., Schneising, O., Rozanov, V., Krings, T.,
500   Burrows, J. P., Boesch, H., Gerbig, C., Meijer, Y. and Loscher, A. : Carbon Monitoring Satellite (CarbonSat):
501   assessment of atmospheric CO2 and CH4 retrieval errors by error parameterization, Atmos. Meas. Tech., 6,
502   3477-3500, 2013.

503 Chevallier, F., Breon, F. M. and Rayner, P. J.: Contribution of the Orbiting Carbon Observatory to the estimation of
504   CO2 sources and sinks: Theoretical study in a variational data assimilation framework, J. Geophys. Res.
505   Atmos., 112, D09307, doi:10.1029/2006JD007375, 2007.

506 Choi, Y. H., Vay, S. A., Vadrevu, K. P., Soja, A. J., Woo, J. H., Nolf, S. R., Sachse, G. W., Diskin, G. S., Blake, D.
507   R., Blake, N. J., Singh, H. B., Avery, M. A., Fried, A., Pfister, L. and Fuelberg, H. E.: Characteristics of the
508   atmospheric CO2 signal as observed over the conterminous United States during INTEX-NA, J. Geophys. Res.
509   Atmos., 113, D07301, doi:10.1029/2007JD008899, 2008.

510 Ciais, P., Rayner, P., Chevallier, F., Bousquet, P., Logan, M., Peylin, P. and Ramonet, M.: Atmospheric inversions
511   for estimating CO2 fluxes: methods and perspectives, Climatic Change, 103, 69-92, 2010.

512 Conway, T. J., Tans, P. P., Waterman, L. S. and Thoning, K. W.: Evidence for interannual variability of the carbon-
513   cycle from the national-oceanic-and-atmospheric-administration climate-monitoring-and-diagnostics-laboratory
514   global-air-sampling-network, J. Geophys. Res. Atmos., 99, 22831-22855, 1994.

515 Crevoisier, C., Sweeney, C., Gloor, M., Sarmiento, J. L. and Tans, P. P.: Regional US carbon sinks from three-
516   dimensional atmospheric CO2 sampling, Proc. Natl. Acad. Sci. U. S. A., 107, 18348-18353, 2010.

517 Crisp, D., Fisher, B. M., O'Dell, C., Frankenberg, C., Basilio, R., Bosch, H., Brown, L. R., Castano, R., Connor, B.,
518   Deutscher, ¨ N. M., Eldering, A., Griffith, D., Gunson, M., Kuze, A., Mandrake, L., McDuffie, J.,
519   Messerschmidt, J., Miller, C. E., Morino, I., Natraj, V., Notholt, J., O'Brien, D. M., Oyafuso, F., Polonsky, I.,
520   Robinson, J., Salawitch, R., Sherlock, V., Smyth, M., Suto, H., Taylor, T. E., Thompson, D. R., Wennberg, P.
521   O., Wunch, D., and Yung, Y. L.: The ACOS CO2 retrieval algorithm − Part II: Global XCO2 data
522   characterization, Atmos. Meas. Tech., 5, 687–707, doi:10.5194/amt-5-687-2012, 2012.

523 Dee, D. P., Uppala, S. M., Simmons, A. J., Berrisford, P., Poli, P., Kobayashi, S., Andrae, U., Balmaseda, M. A.,
524   Balsamo, G., Bauer, P., Bechtold, P., Beljaars, A. C. M., van de Berg, L., Bidlot, J., Bormann, N., Delsol, C.,
525   Dragani, R., Fuentes, M., Geer, A. J., Haimberger, L., Healy, S. B., Hersbach, H., Holm, E. V., Isaksen, L.,
526   Kallberg, P., Kohler, M., Matricardi, M., McNally, A. P., Monge-Sanz, B. M., Morcrette, J. J., Park, B. K.,
527   Peubey, C., de Rosnay, P., Tavolato, C., Thepaut, J. N. and Vitart, F.: The ERA-Interim reanalysis:
528   configuration and performance of the data assimilation system, Q.J.R. Meteorol. Soc., 137, 553-597, 2011.

529 Denning, A. S., Takahashi, T., and Friedlingstein, P.: Can a strong atmospheric CO2 rectifier effect be reconciled
530   with a "reasonable" carbon budget?, Tellus B, 51, 249–253, 1999.

531 Feng, L., Palmer, P. I., Parker, R. J., Deutscher, N. M., Feist, D. G., Kivi, R., Morino, I. and Sussmann, R.:
532   Estimates of European uptake of CO2 inferred from GOSAT X-CO2 retrievals: sensitivity to measurement bias
533   inside and outside Europe, Atmos. Chem. Phys., 16, 1289-1302, 2016.

534 Frankenberg, C., Kulawik, S. S., Wofsy, S., Chevallier, F., Daube, B., Kort, E. A., O'Dell, C., Olsen, E. T., and
535   Osterman, G.: Using airborne HIAPER Pole-to-Pole Observations (HIPPO) to evaluate model and remote
536   sensing estimates of atmospheric carbon dioxide, Atmos. Chem. Phys., , 16, 7867−7878, 2016. doi:10.5194/acp-
537   16-7867-2016, 2016.

538 Gerbig, C., Lin, J. C., Wofsy, S. C., Daube, B. C., Andrews, A. E., Stephens, B. B., Bakwin, P. S. and Grainger, C.
539   A.: Toward constraining regional-scale fluxes of CO2 with atmospheric observations over a continent: 1.
540   Observed spatial variability from airborne platforms J. Geophys. Res. Atmos., 108, doi:10.1029/2002JD003018,
541   2003.

542 Chevallier, F., Palmer, P. I., Feng, L., Boesch, H., O'Dell, C. W., and Bousquet, P.: Towards robust and consistent
543   regional CO_2 flux estimates from in situ and space-borne measurements of atmospheric CO_2, Geophys. Res.
544   Lett., 41, 1065−1070, doi:10.1002/2013GL058772, 2014.

545 Gourdji, S. M., Mueller, K. L., Yadav, V., Huntzinger, D. N., Andrews, A. E., Trudeau, M., Petron, G., Nehrkorn,
546   T., Eluszkiewicz, J., Henderson, J., Wen, D., Lin, J., Fischer, M., Sweeney, C. and Michalak, A. M.: North
547   American CO2 exchange: inter-comparison of modeled estimates with results from a fine-scale atmospheric
548   inversion, Biogeosci., 9, 457-475, 2012

549 Gurney, K. R., Law, R. M., Denning, A. S., Rayner, P. J., Baker, D., Bousquet, P., Bruhwiler, L., Chen, Y. H., Ciais,
550   P., Fan, S., Fung, I. Y., Gloor, M., Heimann, M., Higuchi, K., John, J., Maki, T., Maksyutov, S., Masarie, K.,
551   Peylin, P., Prather, M., Pak, B. C., Randerson, J., Sarmiento, J., Taguchi, S., Takahashi, T. and Yuen, C. W.:
552   Towards robust regional estimates of CO2 sources and sinks using atmospheric transport models, Nature,
553   415(6872), 626-630, 2002.

554 Gurney, K. R., Law, R. M., Denning, A. S., Rayner, P. J., Pak, B. C., Baker, D., Bousquet, P., Bruhwiler, L., Chen,
555   Y. H., Ciais, P., Fung, I. Y., Heimann, M., John, J., Maki, T., Maksyutov, S., Peylin, P., Prather, M. and
556   Taguchi, S.: Transcom 3 inversion intercomparison: Model mean results for the estimation of seasonal carbon
557   sources and sinks, Global Biogeochem. Cycles, 18, GB1010, doi:10.1029/2003GB002111, 2004.

558 Houweling, S., Breon, F. M., Aben, I., Rodenbeck, C., Gloor, M., Heimann, M. and Ciais, P.: Inverse modeling of
559   CO2 sources and sinks using satellite data: a synthetic inter-comparison of measurement techniques and their
560   performance as a function of space and time, Atmos. Chem. Phys., 4, 523-538, 2004.

561 Inoue, M., Morino, I., Uchino, O., Miyamoto, Y., Yoshida, Y., Yokota, T., Machida, T., Sawa, Y., Matsueda, H.,
562   Sweeney, C., Tans, P. P., Andrews, A. E., Biraud, S. C., Tanaka, T., Kawakami, S. and Patra, P. K.: Validation
563   of XCO2 derived from SWIR spectra of GOSAT TANSO-FTS with aircraft measurement data, Atmos. Chem.
564   Phys., 13, 9771-9788, 2013.

565 Inoue, M., Morino, I., Uchino, O., Nakatsuru, T., Yoshida, Y., Yokota, T., Wunch, D., Wennberg, P. O., Roehl, C.
566   M., Griffith, D. W. T., Velazco, V. A., Deutscher, N. M., Warneke, T., Notholt, J., Robinson, J., Sherlock, V.,
567   Hase, F., Blumenstock, T., Rettinger, M., Sussmann, R., Kyrö, E., Kivi, R., Shiomi, K., Kawakami, S., De
568   Mazière, M., Arnold, S. G., Feist, D. G., Barrow, E. A., Barney, J., Dubey, M., Schneider, M., Iraci, L.,
569   Podolske, J. R., Hillyard, P., Machida, T., Sawa, Y., Tsuboi, K., Matsueda, H., Sweeney, C., Tans, P. P.,
570   Andrews, A. E., Biraud, S. C., Fukuyama, Y., Pittman, J. V., Kort, E. A., and Tanaka, T.: Bias corrections of

GOSAT SWIR XCO2 and XCH4 with TCCON data and their evaluation using aircraft measurement data, Atmos. Meas. Tech. 9, 3491–3512, 2016, doi:10.5194/amt-9-3491-2016.

Karion, A., Sweeney, C., Tans, P., and Newberger, T.: AirCore: An Innovative Atmospheric Sampling System, J. Atmos. Ocean. Tech., 27, 1839–1853, doi:10.1175/2010JTECHA1448.1, 2010.

Karion, A., C. Sweeney, S. Wolter, T. Newberger, H. Chen, A. Andrews, J. Kofler, D. Neff, and P. Tans (2013), Long-term greenhouse gas measurements from aircraft, Atmos. Meas. Tech., 6(3), 511–526, doi:10.5194/amt-6-511-2013.

Keeling, C. D. and Rakestraw, N. W.: The concentration of carbon dioxide in the atmosphere, J. Geophys. Res., 65, 2502-2502, 1960.

Keppel-Aleks, G., Wennberg, P. O., Washenfelder, R. A., Wunch, D., Schneider, T., Toon, G. C., Andres, R. J., Blavier, J.-F., Connor, B., Davis, K. J., Desai, A. R., Messerschmidt, J., Notholt, J., Roehl, C. M., Sherlock, V., Stephens, B. B., Vay, S. A., and Wofsy, S. C.: The imprint of surface fluxes and transport on variations in total column carbon dioxide, Biogeosci., 9, 875– 891, doi:10.5194/bg-9-875-2012, 2012.

Kulawik, S. S., Worden, J. R., Wofsy, S. C., Biraud, S. C., Nassar, R., Jones, D. B. A., Olsen, E. T., Jimenez, R., Park, S., Santoni, G. W., Daube, B. C., Pittman, J. V., Stephens, B. B., Kort, E. A., Osterman, G. B. and Team, T. E. S.: Comparison of improved Aura Tropospheric Emission Spectrometer CO2 with HIPPO and SGP aircraft profile measurements, Atmos. Chem. Phys., 13, 3205-3225, 2013.

Lauvaux, T., Schuh, A. E., Uliasz, M., Richardson, S., Miles, N., Andrews, A. E., Sweeney, C., Diaz, L. I., Martins, D., Shepson, P. B. and Davis, K. J.: Constraining the CO2 budget of the corn belt: exploring uncertainties from the assumptions in a mesoscale inverse system, Atmos. Chem. Phys., 12, 337-354, 2012.

Machida, T., Kita, K., Kondo, Y., Blake, D., Kawakami, S., Inoue, G. and Ogawa, T. : Vertical and meridional distributions of the atmospheric CO2 mixing ratio between northern midlatitudes and southern subtropics, J. Geophys. Res. Atmos., 108(D3), 8401, doi:10.1029/2001JD000910, 2002.

Machida, T., Matsueda, H., Sawa, Y., Nakagawa, Y., Hirotani, K., Kondo, N., Goto, K., Nakazawa, T., Ishikawa, K. and Ogawa, T.: Worldwide Measurements of Atmospheric CO2 and Other Trace Gas Species Using Commercial Airlines, J. Atmos. Ocean. Tech., 25(10), 1744-1754, 2008.

Mesinger, F., DiMego, G., Kalnay, E., Mitchell, K., Shafran, P. C., Ebisuzaki, W., Jovic, D., Woollen, J., Rogers, E., Berbery, E. H., Ek, M. B., Fan, Y., Grumbine, R., Higgins, W., Li, H., Lin, Y., Manikin, G., Parrish, D., and Shi, W.: North American regional reanalysis, B. Am. Meteorol. Soc., 87, 343–360, doi:10.1175/BAMS-87-3-343, 2006.

Messerschmidt, J., Geibel, M. C., Blumenstock, T., Chen, H., Deutscher, N. M., Engel, A., Feist, D. G., Gerbig, C., Gisi, M., Hase, F., Katrynski, K., Kolle, O., Lavric, J. V., Notholt, J., Palm, M., Ramonet, M., Rettinger, M., Schmidt, M., Sussmann, R., Toon, G. C., Truong, F., Warneke, T., Wennberg, P. O., Wunch, D. and Xueref-Remy, I.: Calibration of TCCON column-averaged CO2: the first aircraft campaign over European TCCON sites, Atmos. Chem. Phys., 11(21), 10765-10777, 2011.

Miller, C. E., Crisp, D., DeCola, P. L., Olsen, S. C., Randerson, J. T., Michalak, A. M., Alkhaled, A., Rayner, P., Jacob, D. J., Suntharalingam, P., Jones, D. B. A., Denning, A. S., Nicholls, M. E., Doney, S. C., Pawson, S.,

608   Boesch, H., Connor, B. J., Fung, I. Y., O'Brien, D., Salawitch, R. J., Sander, S. P., Sen, B., Tans, P., Toon, G.

609   C., Wennberg, P. O., Wofsy, S. C., Yung, Y. L. and Law, R. M.: Precision requirements for space-based X-CO2

610   data, J. Geophys. Res. Atmos., 112, D10314, doi:10.1029/2006JD007659, 2007.

611 Miller, J. B., Lehman, S. J., Montzka, S. A., Sweeney, C., Miller,B. R., Karion, A., Wolak, C., Dlugokencky, J.,

612   Southon, J., Turnbull, J. C., and Tans, P. P.: Linking emissions of fossil fuel CO2 and other anthropogenic trace

613   gases using atmospheric 14CO2, J. Geophys. Res., 117, D08302, doi:10.1029/2011JD017048, 2012.

614 Miller, S. T. K., Keim, B. D., Talbot, R. W. and Mao, H.: Sea breeze: Structure, forecasting, and impacts, Rev.

615   Geophys., 41, 1011, doi:10.1029/2003RG000124, 2003.

616 Miyamoto, Y., Inoue, M., Morino, I., Uchino, O., Yokota, T., Machida, T., Sawa, Y., Matsueda, H., Sweeney, C.,

617   Tans, P. P., Andrews, A. E. and Patra, P. K.: Atmospheric column-averaged mole fractions of carbon dioxide at

618   53 aircraft measurement sites, Atmos. Chem. Phys., 13(10), 5265-5275, 2013.

619 Peters, W., Jacobson, A. R., Sweeney, C., Andrews, A. E., Conway, T. J., Masarie, K., Miller, J. B., Bruhwiler, L.

620   M. P., Petron, G., Hirsch, A. I., Worthy, D. E. J., van der Werf, G. R., Randerson, J. T., Wennberg, P. O., Krol,

621   M. C. and Tans, P. P.: An atmospheric perspective on North American carbon dioxide exchange:

622   CarbonTracker, Proc. Natl. Acad. Sci. U. S. A., 104(48), 18925-18930, 2007.

623 Ramonet, M., Ciais, P., Nepomniachii, I., Sidorov, K., Neubert, R. E. M., Langendorfer, U., Picard, D., Kazan, V.,

624   Biraud, S., Gusti, M., Kolle, O., Schulze, E. D. and Lloyd, J.: Three years of aircraft-based trace gas

625   measurements over the Fyodorovskoye southern taiga forest, 300 km north-west of Moscow, Tellus B-Chem.

626   Phys. Meteor., 54(5), 713-734, 2002.

627 Reuter, M., Bovensmann, H., Buchwitz, M., Burrows, J. P., Connor, B. J., Deutscher, N. M., Griffith, D. W. T.,

628   Heymann, J., Keppel-Aleks, G., Messerschmidt, J., Notholt, J., Petri, C., Robinson, J., Schneising, O., Sherlock,

629   V., Velazco, V., Warneke, T., Wennberg, P. O. and Wunch, D.: Retrieval of atmospheric CO2 with enhanced

630   accuracy and precision from SCIAMACHY: Validation with FTS measurements and comparison with model

631   results, J. Geophys. Res. Atmos., 116, 2011.

632 Reuter, M., Buchwitz, M., Hilker, M., Heymann, J., Schneising, O., Pillai, D., Bovensmann, H., Burrows, J. P.,

633   Bosch, H., Parker, R., Butz, A., Hasekamp, O., O'Dell, C. W., Yoshida, Y., Gerbig, C., Nehrkorn, T.,

634   Deutscher, N. M., Warneke, T., Notholt, J., Hase, F., Kivi, R., Sussmann, R., Machida, T., Matsueda, H. and

635   Sawa, Y.: Satellite-inferred European carbon sink larger than expected, Atmos. Chem. Phys., 14(24), 13739-

636   13753, 2014.

637 Reuter, M., Buchwitz, M., Hilker, M., Heymann, J., Bovensmann, H., Burrows, J. P., Houweling, S., Liu, Y. Y.,

638   Nassar, F., Chevallier, F., Cias, P., Marshall, J., and Reichstein, M.: How much CO2 is taken up by the

639   European terrestrial biosphere? Bull. Am. Meteor. Soc., 98, 665–671, doi:10.1175/BAMS-D-15-00310.1, 2017.

640 Saitoh, N., Kimoto, S., Sugimura, R., Imasu, R., Kawakami, S., Shiomi, K., Kuze, A., Machida, T., Sawa, Y. and

641   Matsueda, H.: Algorithm update of the GOSAT/TANSO-FTS thermal infrared CO2 product (version 1) and

642   validation of the UTLS CO2 data using CONTRAIL measurements, Atmos. Meas. Tech., 9(5), 2119-2134,

643   2016.

644 Stephens, B. B., Gurney, K. R., Tans, P. P., Sweeney, C., Peters, W., Bruhwiler, L., Ciais, P., Ramonet, M.,
645   Bousquet, P., Nakazawa, T., Aoki, S., Machida, T., Inoue, G., Vinnichenko, N., Lloyd, J., Jordan, A., Heimann,
646   M., Shibistova, O., Langenfelds, R. L., Steele, L. P., Francey, R. J. and Denning, A. S.: Weak northern and
647   strong tropical land carbon uptake from vertical profiles of atmospheric CO(2), Science, 316(5832), 1732-1735,
648   2007.

649 Sweeney, C., Karion, A., Wolter, S., Newberger, T., Guenther, D., Higgs, J. A., Andrews, A. E., Lang, P. M., Neff,
650   D., Dlugokencky, E., Miller, J. B., Montzka, S. A., Miller, B. R., Masarie, K. A., Biraud, S. C., Novelli, P. C.,
651   Crotwell, M., Crotwell, A. M., Thoning, K. and Tans, P. P.: Seasonal climatology of CO2 across North America
652   from aircraft measurements in the NOAA/ESRL Global Greenhouse Gas Reference Network, J. Geophys. Res.
653   Atmos., 120(10), 5155-5190, 2015.

654 Tanaka, M., Nakazawa, T. and Aoki, S.: Concentration of atmospheric carbon-dioxide over japan, J. Geophys. Res.
655   Ocean., 88(C2), 1339-1344, DOI: 10.1029/JC088iC02p01339, 1983.

656 Tanaka, T., Miyamoto, Y., Morino, I., Machida, T., Nagahama, T., Sawa, Y., Matsueda, H., Wunch, D., Kawakami,
657   S. and Uchino, O.: Aircraft measurements of carbon dioxide and methane for the calibration of ground-based
658   high-resolution Fourier Transform Spectrometers and a comparison to GOSAT data measured over Tsukuba
659   and Moshiri, Atmos. Meas. Tech., 5(8), 2003-2012, 2012.

660 Tans, P. P., Conway, T. J. and Nakazawa, T.: Latitudinal distribution of the sources and sinks of atmospheric
661   carbon-dioxide derived from surface observations and an atmospheric transport model, J. Geophys. Res.
662   Atmos., 94(D4), 5151-5172, 1989.

663 Tans, P. P., Fung, I. Y. and Takahashi, T.: Observational constraints on the global atmospheric co2 budget, Science,
664   247(4949), 1431-1438, 1990.

665 Thoning, K. W., Tans, P. P. and Komhyr, W. D.: Atmospheric carbon-dioxide at Mauna Loa observatory. 2.
666   Analysis of the NOAA GMCC data, 1974-1985, J. Geophys. Res. Atmos., 94(D6), 8549-8565, 1989.

667 Washenfelder, R. A., Toon, G. C., Blavier, J. F., Yang, Z., Allen, N. T., Wennberg, P. O., Vay, S. A., Matross, D.
668   M. and Daube, B. C.: Carbon dioxide column abundances at the Wisconsin Tall Tower site, J. Geophys. Res.
669   Atmos., 111, D22305, doi:10.1029/2006JD00715,4 2006.

670 Wofsy, S. C.: HIAPER Pole-to-Pole Observations (HIPPO): finegrained, global-scale measurements of climatically
671   important atmospheric gases and aerosols, Philos. T. R. Soc. A, 369, 2073–2086, doi:10.1098/rsta.2010.0313,
672   2011.

673 Wunch, D., Wennberg, P. O., Toon, G. C., Keppel-Aleks, G., and Yavin Y. G.: Emissions of greenhouse gases from
674   a North American megacity, Geophys. Res. Lett., 36, L15810, doi:10.1029/2009GL039825, 2009.

675 Wunch, D., Toon, G. C., Wennberg, P. O., Wofsy, S. C., Stephens, B. B., Fischer, M. L., Uchino, O., Abshire, J. B.,
676   Bernath, P., Biraud, S. C., Blavier, J. F. L., Boone, C., Bowman, K. P., Browell, E. V., Campos, T., Connor, B.
677   J., Daube, B. C., Deutscher, N. M., Diao, M., Elkins, J. W., Gerbig, C., Gottlieb, E., Griffith, D. W. T., Hurst,
678   D. F., Jimenez, R., Keppel-Aleks, G., Kort, E. A., Macatangay, R., Machida, T., Matsueda, H., Moore, F.,
679   Morino, I., Park, S., Robinson, J., Roehl, C. M., Sawa, Y., Sherlock, V., Sweeney, C., Tanaka, T. and Zondlo,

680   M. A.: Calibration of the Total Carbon Column Observing Network using aircraft profile data', Atmos. Meas.
681   Tech., 3(5), 1351-1362, 2010.

682 Wunch, D., Toon, G. C., Blavier, J.-F. L., Washenfelder, R. A., Notholt, J., Connor, B. J., Griffith, D. W. T.,
683   Sherlock, V., and Wennberg, P. O.: The total carbon column observing network, Philosophical Transactions of
684   the Royal Society - Series A: Mathematical, Physical and Engineering Sciences, 369(1943), 2087-2112,
685   doi:10.1098/rsta.2010.0240, 2011.

686 Wunch, D., Wennberg, P. O., Messerschmidt, J., Parazoo, N. C., Toon, G. C., Deutscher, N. M., Keppel-Aleks, G.,
687   Roehl, C. M., Randerson, J. T., Warneke, T., and Notholt, J.: The covariation of Northern Hemisphere
688   summertime CO_2 with surface temperature in boreal regions, Atmos. Chem. Phys., 13, 9447–9459,
689   doi:10.5194/acp-13-9447-2013, 2013.